Combining Local Binary Pattern with Stationary Wavelet Transform for Multiclass Classification of Brain Disorders

Vandana V. Kale[1] , Pritesh Shah[2*] , Ravi Sekhar[2] , Chandrakant R. Sonawane[2] , Anand Pandey[2] , Durgesh Nandan[3]

[1] Department of Instrumentation Engineering, AISSMS's Institute of Information Technology, Pune 411001, India
[2] Symbiosis Institute of Technology, Pune Campus, Symbiosis International (Deemed University) (SIU), Pune 412115, India
[3] School of CS&AI, SR University, Warangal 506371, Telangana, India

Corresponding Author Email: pritesh.shah@sitpune.edu.in

ABSTRACT

Neurological disorders affect the brain, spine and nervous system. Many neurological disorders result in substantial morbidity, therefore early and accurate diagnosis is necessary for rehabilitation. This study proposes a brain abnormality descriptor using local binary pattern and stationary wavelet transform (LBP-SWT). LBP depicts the local structure of MR brain image and SWT coefficients provide multi-scale directional representation for brain abnormalities encoded in the extracted LBP. Three features namely energy, Shannon entropy and standard deviation are calculated from LBP-SWT decomposed subbands. For binary and multi-class disorder classification, four datasets are used. Cross-validation is employed with the backpropagation neural network (BPNN) classifier. Among three features, standard deviation achieved highest binary classification average accuracy of 100%, 100%, 99.84% and 99.04% and multi-class classification average accuracy of 98.08%, 97.83%, 95.97% and 92.78% on (Dataset)DS:66, DS:160, DS:255, and DS:612 datasets respectively. Also, experimentation is carried out on 1836 images obtained by rotating and translating the images of dataset DS:612. For dataset, DS:1836, the standard deviation achieved the highest multi-disease classification average accuracy of 92.32%. The comparative results using three features show the standard deviation feature has more discriminating capacity than energy and Shannon entropy. The experimental results reveal improvement in the proposed work regarding evaluation metrics compared with state-of-the-art methods. In this paper, we proposed LBP-SWT approach to generate affluent representation of brain image whose features have more discriminating power to categorize brain disorders. The translation invariant feature of SWT contributes in LBP-SWT approach in accurate diagnosis of shifted brain images also. It is useful in clinical applications.

1. INTRODUCTION

The diagnosis of different disorders is the most important step in deciding the treatment for the disease. Recently, brain disorders that strike at different phases of human life are among society's most severe pathological states. Various imaging techniques and methods have emerged for brain disease identification. The approaches using wavelets are widely used in different image processing and diagnosis applications [1, 2]. The structural MRI modality presents brain disorders non-invasively and with better contrast [3]. However, the capacious MR imaging data can be arduous to interpret manually. Therefore, computer aided detection (CAD) systems are being developed to help physicians in the interpretation of medical images, resulting in improved diagnostic accuracy. Various CAD systems have been proposed by researchers for classifying normal and abnormal MR brain images. Zhang et al. [4] used wavelet coefficients and BPNN classifier for classification of brain disorders, and the study [5] developed an algorithm using ripplet transform (RT) along with multi-scale geometric analysis. They utilized the least square support vector machine for classification. El-Dahshan et al. [6] segmented MR images using feedback pulse-coupled neural networks. The study [7] achieved 97.78% classification accuracy over 90 MR images using wavelet energy as a feature and support vector machine (SVM) classifier. Zhang et al. [8] calculated wavelet entropy of approximation wavelet coefficients and used BBO and PSO to optimize NN for classification. Zhang et al. [9] extracted SWT coefficients from MR images. The features were classified using a variant of the SVM classifier. Wang et al. [10] utilized a twin SVM classifier to classify the extracted dual-tree complex wavelet transform features. Wang et al. [11] reduced the stationary wavelet transform (SWT) coefficients using PCA. They proposed a classifier using variants of feed-forward neural network (FNN) based on hybridization

methods of PSO and ABC. Zhang et al. [12] classified the entropies of wavelet packet transform coefficients using generalized eigenvalue proximal SVM (GEPSVM). In the study [13], wavelet entropy (WE) feature was calculated from approximation and detail wavelet coefficients. Features were selected using binary particle swarm optimization (BPSO) and its variants. Nayak et al. [14] employed probabilistic PCA (PPCA) to reduce the 2D DWT coefficients and perform classification using Adaboost algorithm with random forest (ADBRF). Nayak et al. [15] used energy and entropy values, calculated from SWT coefficients, as features. They employed Adaboost algorithm with SVM classifier. Nayak et al. [16] classified MR brain images using curvelet features and three kernels in the least squares SVM classifier. They described promising results. Khalil et al. [17] employed various features, such as local binary pattern (LBP), gray level co-occurrence matrix (GLCM), and histogram of oriented gradient (HOG). They combined the classifiers of these feature extraction techniques using different fusion operators. Gudigar et al. [18] compared three different multi-resolution analysis techniques to classify a dataset of 612 MR brain images using SVM as a classifier and achieved 97.38% accuracy with shearlet coefficients.

Nayak et al. [19] proposed transfer learning approach and Tamilarasiand and Gopinathan [20] proposed Inception Architecture for brain abnormalities detection. Hu et al. [21] explored the approach of fuzzy system for feature recognition and predicting the brain disease. Shanker and Bhattacharya [22] segmented region of interest of MR brain images using their developed Pulse-Coupled Neural Network and classified the brain images using Twin Support Vector Machine. Convolutional neural networks are being widely used in biomedical image examination [23]. Takrouni and Douik [24] combined Curvelet Pooling (CP) and Adam gradient calculation method for improving classification accuracy of brain pathological images. Dora et al. [25] suggested multiple kernel-based convolutional neural network (MK-CNN) to classify the pathological brain images, which is a flexible and high-capacity approach. Zhou et al. [26] addressed the dual challenges of data privacy and MRI brain tumor disease detection using an innovative approach of leveraging Federated Learning (FL). Akter et al. [27] proposed a model using deep Convolutional Neural Network (CNN) for automatic brain image classification and a U-Net-based segmentation. Kale et al. [28] suggested new feature extraction method using local binary pattern and steerable pyramid (SP) and then MR brain images were classified using neural network.

The literature review reveals that wavelet-related transforms are the most widely used feature extraction methods in CAD systems. The multi-resolution property of these transforms retains significant information about images. PCA is the extensively employed feature reduction method whereas SVM, ANN, and KNN are used as classifiers in most of the work. In these works, promising accuracies are achieved. However, the number of images used in these methods is small; therefore, Gudigar et al. [18] introduced a new dataset DS:612 compromising 612 MR images.

In this paper, we compared the classifier performance results using three features individually. The following is the contribution of this work:

• MR image is encoded in local binary pattern using LBP. The wavelet coefficients of LBP coded image are extracted using SWT. The statistical feature of SWT coefficients give

multi scale directional representation for brain abnormalities encoded in the LBP transformed image.

• 612 images of dataset DS:612 are rotated and translated by different angles and coordinates respectively to obtain dataset DS:1836 of 1836 images.

• Energy, entropy and standard deviation values of each multi scale sub band of LBP-SWT decomposed image are calculated.

• The performance measures of the back propagation neural network classifier are compared using each feature individually over all datasets.

By performing cross-validation with the Harvard Medical School Datasets [29], the proposed method achieved promising performance for binary and multi-class disease classification. The article is arranged as follow. Section 2 presents material. Methodology of presented system is delineated in Section 3. Section 4 highlights the results along with discussion, leading to conclusion in Section 5.

2. MATERIAL

Datasets from the Harvard Medical School website [29] are taken for evaluation purpose. The website contains brain images of various disorders under category of stroke, tumour, degenerative disease, infectious disease. The images available are of imaging modalities like MRI (T1 weighted, T2 weighted and proton density (PD) weighted), computed tomography (CT) or single-photon emission computed tomography (SPECT).
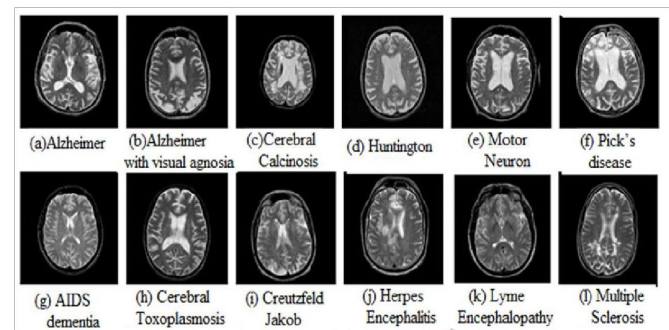
Figure 1. Brain MRI image samples: (a) Alzheimer, (b) Alzheimer with visual agnosia, (c) Cerebral Calcinosis, (d) Huntington, (e) Motor Neuron, (f) Pick's disease, (g) AIDS dementia, (h) Cerebral Toxoplasmosis, (i) Creutzfeld-Jakob, (j) Herpes encephalitis, (k) Lyme encephalopathy, (l) Multiple sclerosis

Table 1. Harvard Medical School datasets: Distribution of normal and abnormal images

Title of Dataset	Count of Total Images	Count of Normal Images	Count of Pathological Images	Count of Brain Disorders
DS:66	66	18	48	7
DS:160	160	20	140	7
DS:255	255	35	220	11
DS:612	612	83	529	24

In state-of-the-art techniques, datasets with 66(DS:66), 160(DS:160) and 255(DS:255) MRI images of size 256×256 resolution and T2-weighted are extensively used. Datasets DS: 160 and DS: 66 contain brain disorders namely Pick's disease,

Alzheimer, Huntington, Alzheimer's disease plus visual agnosia, Glioma, Meningioma, and Sarcoma. Additional abnormalities namely Herpes encephalitis, Multiple sclerosis, Chronic subdural, and Cerebral toxoplasmosis hematoma have been included in Dataset DS:255. Gudigar et al. [18] introduced a new dataset DS:612. Further, thirteen new abnormal medical data types are included in dataset DS:612 resulting in a total of twenty-four brain abnormalities. Sample MR brain images are shown in Figure 1. The distribution of normal and pathological images of the datasets used in this work is given in Table 1.

3. METHODOLOGY

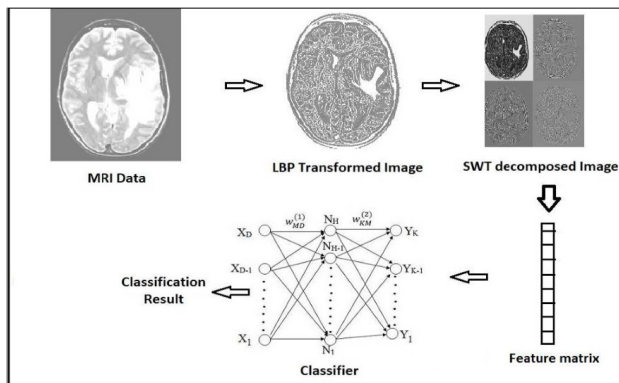The methodology of proposed feature extraction and classification system is summarized in Figure 2.

Figure 2. Proposed feature extraction and classification method

3.1 Local binary pattern (LBP)

LBP operator is applied to each MR image. A small cell size of 3×3 is selected, as local abnormalities can be detected effectively with a smaller size.

LBP computes binary code of each pixel. In 3×3 neighbourhood, the LBP code of central pixel is calculated by following equations,

$$LBP_{P,R} = \sum_{p=0}^{p-1} (s(g_p - g_c))2^p \qquad (1)$$

$$s(x) = 0, \quad for\ x < 0; \\ \quad\quad 1, \quad for\ x >= 0 \qquad (2)$$

where, (P, R) specifies a neighbourhood of P, equally spaced points on a circle of radius R, $s(x)$ is the thresholding function, g_c is the centre pixel and $p = 0, 1,...., p-1$ are the pixels in the neighbourhood.

3.2 Stationary wavelet transforms (SWT)

The lack of translation invariance of the DWT is overcome in SWT. This is accomplished by removing the down samplers and up samplers in the DWT and up-sampling the filter coefficients. Due to this property, it is used in various applications despite being redundant [9, 15]. Figure 3 describes decomposition steps of image using 2D-SWT. At level j, 2D-SWT decomposes approximation coefficients (cAj)

in four components namely the approximation coefficients (cAj+1), and the details (horizontal (cDhj+1), vertical (cDvj+1), and diagonal (cDdj+1)) in three orientations. The merits of SWT are shift invariance and it also removes the limitation of size constrains of standard DWT (power of 2). As SWT does not use decimation operation, it can be applied to image of any size.
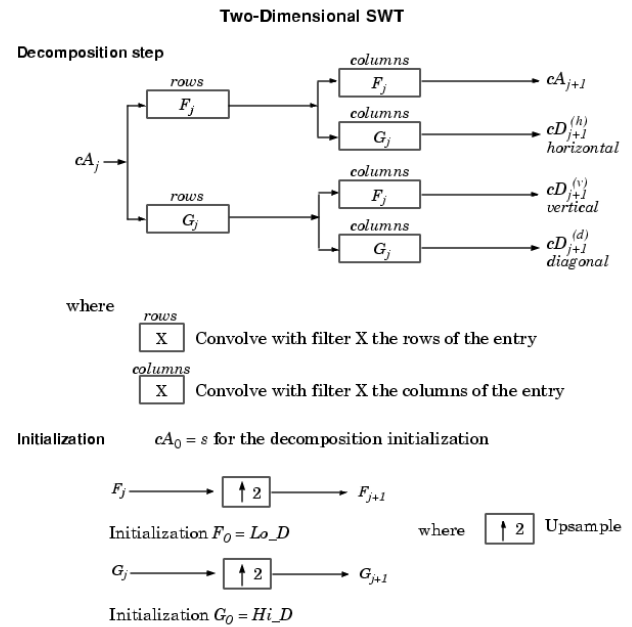

Figure 3. Decomposition steps of image using SWT

3.3 LBP-SWT approach

Wavelet transform (WT) has been used in combination with LBP to describe texture images [30-33]. In most of the applications, wavelet-decomposed sub-bands are used from which LBP features are extracted. In this paper, LBP [34] is used with SWT to provide a robust brain disease descriptor. In this work, the wavelet used is Symlet2. Its smaller compact support is useful in detecting smaller changes in the image. SWT is applied on LBP-transformed image and decomposition is carried out to level 8. The 4 sub-bands namely approximation, horizontal, vertical, and diagonal of each decomposition level contribute to a total of 32 sub-bands. All 32 sub-bands are considered for feature calculation. The LBP-SWT approach combines the power of LBP as a local texture descriptor and the power of the SWT in detecting spatial changes.

3.4 Feature extraction

Feature represents measure of image structure. In this work, three features namely energy, Shannon entropy, and standard deviation are calculated from 32 multi-scale directional sub-bands of the LBP-SWT image. The features are tabulated in Table 2. In Table 2, $X_k (i, j)$ indicates the kth sub-band and its dimension is $M \times N$. k varies from 1 to 8. μk indicates mean of kth sub-band. Energy quantifies the strength of the image details in different sub-bands. As an individual feature, it has been shown to be effective in analysis of MR brain images [7, 35]. Entropy reflects randomness and in turn complexity within brain image. In the classification of normal and abnormal MR brain images [15, 36, 37], entropy feature has

been proved to be competent. Standard deviation provides dispersion measure of coefficient values around mean. It has been used in different applications [38, 39]. The discriminating power of these features varies with the different resolution levels of the image. Such a multi-scale resolution strategy is useful for pattern recognition, and classification [40]. This work, evaluates the competency of these three features in differentiating brain disorders.

Table 2. Feature formula

Feature	Formula
Energy	$\sum_{i=1}^{M}\sum_{j=1}^{N}(X_k(i,j))^2$
Standard deviation	$\sqrt{\dfrac{\sum_i\sum_j(X_k(i,j)-\mu_k)^2}{M\times N}}$
Shannon entropy	$-\sum_i\sum_j(X_k(i,j))^2\,log_2(X_k(i,j))^2$

3.5 Back propagation neural network (BPNN) Classifier

To perform the classification, a supervised learning method, BPNN is used. It is biologically inspired [41]. It can generalize to new using past examples. With these properties, it has achieved considerable success when it is used to solve multivariate, difficult, non-linear, and diverse problems [41-43]. Ojha et al. [44] have given a very good review of the neural network. Optimal selection of hidden layers and also hidden neurons is a crucial part of NN architecture design as it can lead to under-fitting or over-fitting issues. In this work, to overcome the generalization and over-fitting problem of BPNN, the Bayesian regularization method is proposed along with stratified cross-validation. For binary classification, one hidden layer with 5 neurons is used. In multi-class classification, the increase in the number of classes to distinguish, results in increased training equations. So, BPNN with 5 hidden neurons can cause under-fitting issues. To overcome this issue, one hidden layer with 15 neurons is used in multi-class classification for the first three datasets.

4. EXPERIMENTAL RESULTS AND DISCUSSION

Experimentation has been performed on a system with 4 GB of RAM and core i5 (1.60 GHz), for validation of the proposed method under MATLAB environment. The proposed method was evaluated using binary and multi-class disease classifications. The accuracy (ACC), sensitivity (SEN), specificity (SPE) and precision (PRE) were used as performance measures.

4.1 Multi-class disease classification

In multi-class disease classification, the transform techniques namely SWT, LBP-SWT and SWT-LBP were employed with three features energy, Shannon entropy and standard deviation individually to evaluate the classification performance. In SWT approach, MR image was decomposed using SWT only. With LBP-SWT technique, initially image was coded using LBP code and afterwards SWT was used to decompose LBP coded image into LBP-SWT sub-bands. In SWT-LBP approach, the operations were in reverse order as compared with LBP-SWT approach.

All the three techniques with three features were evaluated using datasets DS:66, DS:160, DS:255, DS:612 and DS:1836. DS:1836 contains translated and rotated versions of images of DS:612.

4.1.1 Rotated and translated form of images of DS:612

Dataset DS:612 is having the largest number of images. These images were translated and rotated to form a new dataset DS:1836 of 1836 images. The 612 images of dataset DS:612 were rotated by angles 45°, 90° and 120° and translated by co-ordinates [22, 13], [0, -14.3] and [-7.5, -14.7] respectively to form testing dataset. Similarly, 612 images of dataset DS:612 were rotated by angles 0°, 20° and 70° and translated by co-ordinates [5, 8], [-12, -4.3] and [15, -10] respectively to form training dataset. The dataset DS:1836 consists of 1836 images. The rotation angles and translation co-ordinates were selected randomly. The details are given in Table 3. The sample images of rotated and translated form of original images are shown in Figure 4.

Table 3. Rotation and translation parameters of dataset DS:1836

Testing Dataset		Training Dataset	
Rotation angle [degree]	Translation co-ordinates [x, y]	Rotation angle [degree]	Translation co-ordinates [x, y]
45°	[22, 13]	0°	[5, 8]
90°	[0, -14.3]	20°	[-12, -4.3]
120°	[-7.5, -14.7]	70°	[15, -10]
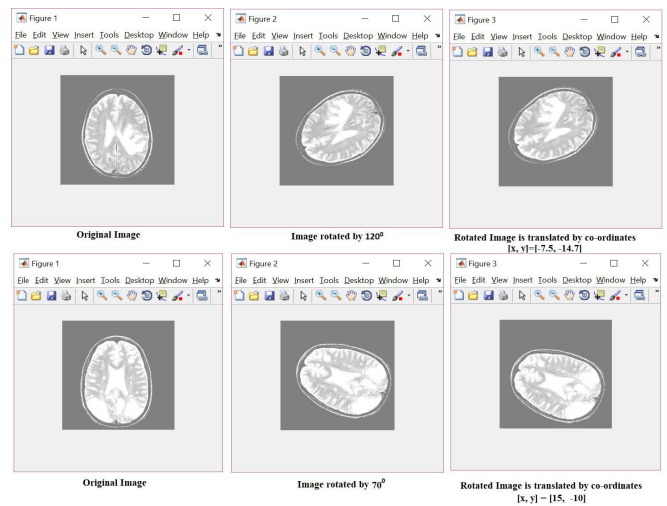
Figure 4. Samples of rotated and translated form of original images of dataset DS:612

4.1.2 Evaluation of classification performance using different transforms and different features

The classification performance accuracy values for multi-class disease classification using three transform techniques, three features and five datasets are presented in Table 4. For fair comparison purpose, the training and test samples were kept same for each method during every run. The average test accuracy values obtained over 5-runs are given in Table 4. Table 4 reveals that the LBP-SWT approach yielded the highest accuracy values using all three features than the counter approaches. The results obtained using SWT method are competent with LBP-SWT method. However, if the order of operation of LBP and SWT is reversed then with SWT-LBP approach, the accuracy results differ considerably. With LBP-

SWT approach, the standard deviation feature attained the maximum test accuracy values of 97.22%, 96.08%, 95.22%, 91.55 and 90.81% for datasets DS:66, DS:160, DS:255, DS:612 and DS:1836. The other two features namely energy and entropy proved to be more effective with LBP-SWT approach than the remaining two approaches namely SWT and

SWT-LBP. Also, the LBP-SWT-std + BPNN method generalized well on dataset DS:1836 having larger number of images than other datasets. Therefore, for in further experimentations LBP-SWT-std + BPNN approach was employed.

Table 4. Performance measures using different transforms, different features and BPNN classifier of multi-class classification

| Methods	Datasets				
	DS:66	DS:160	DS:255	DS:612	DS: 1836
	Avg. Test Accuracy (%)				
LBP-SWT-energy+BPNN	95.10	95.84	94.70	91.02	83.46
LBP-SWT-entropy+BPNN	96.60	95.24	93.39	90.88	87.03
LBP-SWT-std+BPNN	97.22	96.08	95.22	91.55	90.81
SWT-LBP-energy+BPNN	73.13	65.00	54.80	60.42	64.37
SWT-LBP-entropy+BPNN	83.47	80.63	76.49	62.87	61.26
SWT-LBP-std+BPNN	86.81	84.00	78.55	62.00	59.43
SWT-energy+BPNN	95.21	86.13	93.67	82.98	86.66
SWT-entropy+BPNN	93.54	90.25	91.08	84.43	89.89
SWT-std+BPNN	93.75	87.13	93.00	84.32	86.42

4.1.3 Performance results of class wise classification accuracy

The class wise classification accuracy was calculated for all the datasets. The plots of average classification accuracies and average standard deviation in accuracy values are plotted in the following figures. As shown in Figure 5, Glioma, Pick's disease, Huntington and Sarcoma brain diseases are identified with 100% accuracy.
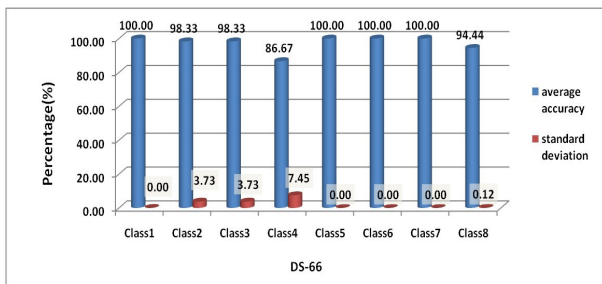
Figure 5. Class wise classification accuracy of dataset DS:66

As shown in Figure 6, Glioma, Alzheimer's disease plus visual agnosia, Huntington and Sarcoma brain diseases are identified with 100% accuracy. As shown in Figure 7, Glioma, Alzheimer's disease plus visual agnosia and Huntington brain diseases are identified with 100% accuracy. As shown in Figure 8, Glioma and Huntington brain diseases are identified with 100% accuracy. As shown in Figure 9, Huntington brain diseases are identified with 100% accuracy.
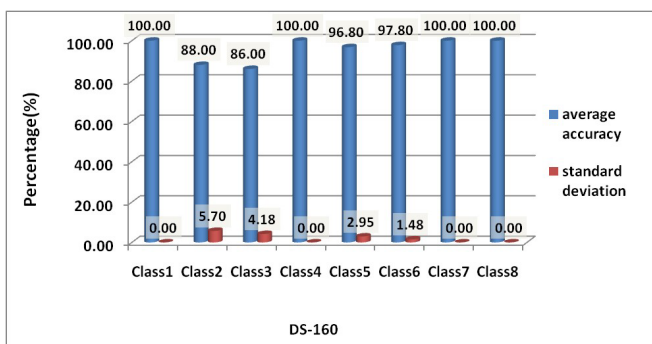
Figure 6. Class wise classification accuracy of dataset DS:160
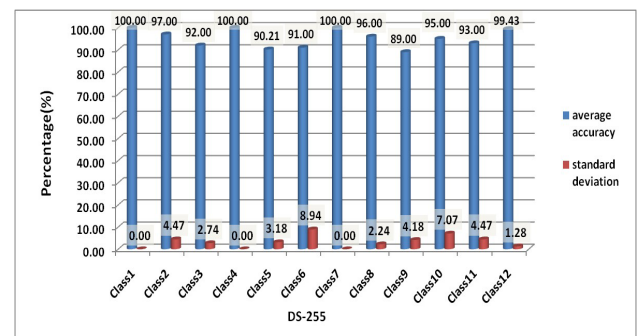
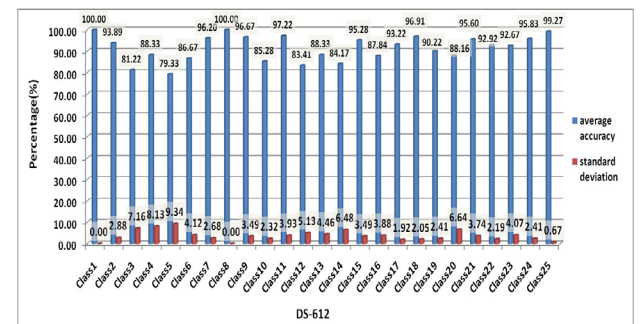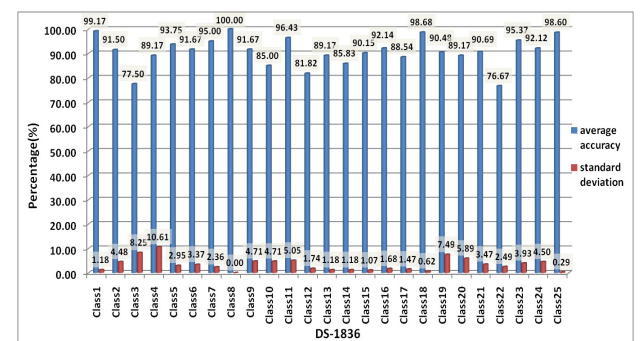**Figure 7.** Class wise classification accuracy of dataset DS:255

Figure 8. Class wise classification accuracy of dataset DS:612

Figure 9. Class wise classification accuracy of dataset DS:1836

4.2 Binary classification

The performance measures for binary classification over four datasets were calculated using (LBP-SWT-std + BPNN) method. The results are given in Table 5. For dataset DS:66, with each feature the classifier could reach up to 100% accuracy, 100% sensitivity and 100% specificity in testing and training phase, as number of images is small. With increasing number of images of datasets DS:160, DS:255 and DS:612, feature standard deviation achieved better performance measures than energy and entropy. For dataset DS:612 having largest number of images, features energy and entropy could not model the training data with 100% accuracy and both of them results in poor performance measures as compared to standard deviation. In brief, for all datasets, standard deviation provides better results than energy and entropy.

Table 5. Comparison of performance measures using different features and BPNN classifier for binary classification

	Datasets	Features	Testing Performance Measures			
			ACC (%)	SEN (%)	SPE (%)	PRE (%)
Classification	DS:66	Energy	100	100	100	100
		Standard Deviation	100	100	100	100
		Entropy	100	100	100	100
	DS:160	Energy	99.63	99.57	100	100
		Standard Deviation	100	100	100	100
		Entropy	99.50	99.43	100	100
	DS:255	Energy	99.61	99.94	97.52	99.61
		Standard Deviation	99.84	99.94	99.24	100
Binary		Entropy	99.61	100	97.14	99.56
	DS:612	Energy	98.79	98.90	98.04	99.7
		Standard Deviation	99.04	99.24	97.78	99.65
		Entropy	98.92	99.11	97.75	99.65

Table 6. Comparison with existing binary classification approaches

Paper	Method	Images	Accuracy (%)
[4]	DWT + PCA +BPNN	66	100
[5]	RT+MGA+PCA+LS-SVM	255	99.39
[6]	FP-CNN + DWT + PCA + BPNN	101	99
[7]	DWT + BBO+ SVM	90	97.78
[8]	DWT + BBO-PSO + ANN	255	99.49
[9]	SWT + PCA + GEPSVM	255	99.41
[10]	DT-CWT+ twin SVM	255	99.57
[11]	SWT+PCA+HPA-FNN	255	99.45
[12]	DWT +GEPSVM	255	99.33
[13]	WE+BPSO+PNN	255	99.53
[14]	DWT+PPCA+ADBRF	255	99.53
[15]	SWT+ADBSVM	255	99.45
[16]	Curvelet transform+PCA+SVM	255	99.61
[17]	Combined Operator	160	100
[18]	Shearlet transform + PSO + SVM	612	97.38
Proposed	LBP + SWT + Std + BPNN	66	100
		160	100
		255	99.84
		612	99.04

4.3 Comparison with existing classification methods

4.3.1 Binary classification

In this section, the results of proposed work are compared with state-of-the-art techniques and tabulated in Table 6. In the existing methods, the researchers achieved 100% accuracy in case of widely used datasets DS:66 and DS:160. Also, promising accuracies are achieved for DS:255. However, the number of images used in these methods are small, so the study [18] introduced new dataset DS:612 consisting of 612 images. With our proposed method, we achieved higher accuracy of 99.84% and 99.04% for datasets DS:255 and DS:612 respectively than existing methods.

The studies [7, 8, 10, 12, 15] utilised WT and its variants and wavelets used were Haar and Db-4. Using these techniques, they decomposed MR images to the maximum level of 6 and they calculated statistical features like energy, entropy or variants over the decomposed sub-bands.

Some of the methods [16, 18] employed transform techniques other than DWT namely Curvelet, Shearlet transforms and achieved promising results. In the proposed method, we used Symlet2 wavelet. Its's smaller compact support is useful in detecting smaller changes in the image. Selection of wavelet Symlet2 (which can detect smaller changes in images), the transform technique SWT (which contains all the coefficients and the information is retained) and statistical values calculated over decomposed sub-bands compositely resulted in achieving better performance results than state of-the-art methods. We compared other performance measures with dataset DS:612. Table 7 shows that along with accuracy, sensitivity and specificity values are also increased in our proposed method as compare to dataset DS:612 of the study [18].

4.3.2 Multi-class classification

The wavelet multi-class classification is more complex than

binary classification and is relatively less considered in the previous studies. However, the diagnosis of disease type is very important to provide correct treatment. Table 8 summarizes the multi-class classification results of state-of-the-art methods. The study [45] used deep neural network to classify the wavelet extracted features of 4 different types of MR images and they achieved accuracy of 96.97% on 66 images. The study [46] employed DWT to extract features and random forest as classifier. They attained 95.70% accuracy while classifying 6 classes of 310 MR images. However, with our proposed system, we achieved higher accuracy of 96.52%

than the study [46]. The studies [45, 46] employed DWT technique using Haar wavelet and decomposed images to level 3. Further, they reduced the approximate coefficients at level 3 using PCA. We could reach up to 97.22%, 96.08%, 95.22%, 96.52% and 91.55% accuracies using 66, 160, 255, 310 and 612 MR images incorporating 8,8,12,6 and 25 different MR brain image classes respectively. Table 8 depicts that with increase in the number of images and classes to distinguish, our proposed system attained better results than the existing methods.

Table 7. Comparison of performance measures of existing technique with dataset DS:612

Method	Images	ACC (%)	SEN (%)	SPE (%)
Gudigar et al. [18]: Shearlet transform + PSO + SVM	612	97.38	99.05	80.69
Proposed method: LBP + SWT + Std + BPNN	612	99.04	99.24	97.78

Table 8. Result of multi-class disease classification

| Paper	Method	Total Images	Brain Disorders	Total Number of Classes	Accuracy (%)
[45]	DWT + PCA + DNN	66	3	4	96.97
[46]	DWT + PCA + RF	310	5	6	95.70
		66	7	8	97.22
		160	7	8	96.08
Proposed method	LBP + SWT + Std + BPNN	255	11	12	95.22
		310	5	6	96.52
		612	24	25	91.55

Table 9. Comparison of performance measure of BPNN architectures for dataset DS:612

Classification	Features	Testing Phase ACC (%)		
		In-15-10-Out	In-20-15-Out	In-20-20-Out
Multi-class	Energy	86.05	89.77	91.02
	Standard Deviation	86.08	90.98	91.55
	Entropy	84.25	89.58	90.88

4.4 Experimentation on dataset DS:612

4.4.1 BPNN architecture

In multi-class classification for Dataset DS:612, total 612 images were classified into 25 types of MR brain images.
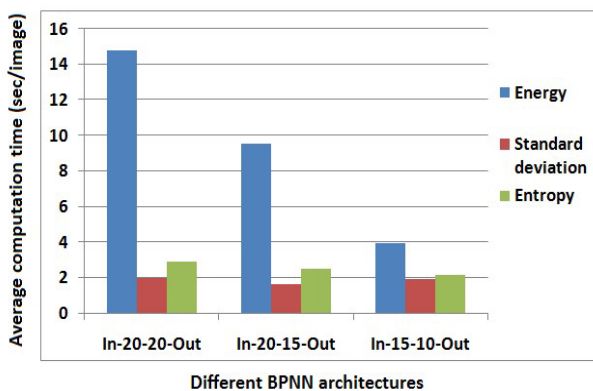
Figure 10. Average computation time for multi-class classification by using different BPNN architectures and features for dataset DS:612

The resulting number of training equations was very large, so a single hidden layer with 15 neurons, which could achieve better results for other three datasets, could not model training data of DS:612 efficiently. So, two hidden layers with different

combinations of neurons in first and second layer were tested. The hidden neurons combinations and their performance measures are tabulated in Table 9, which indicates input layer neurons and out indicates output layer neurons. Table 9 depicts that, with 20 hidden neurons in each layer, BPNN attained highest testing accuracy of 91.55% using standard deviation feature. The Bayesian regularization algorithm conquer the over fitting issue.

All the three features achieved comparable accuracy in Training phase but the computation time required by energy feature is the largest and by standard deviation is the least. The computation time analysis is shown in Figure 10. The average computation for one image is 14.77 sec, 1.94 sec and 2.91 sec using energy, standard deviation and entropy feature respectively.

4.5 Discussion

The comparative results tabulated in Table 4, reveal that the LBP-SWT approach yielded the highest accuracy values using all three features than the counter methods, SWT and SWT-LBP. With the LBP-SWT approach, the standard deviation feature attained more classification accuracy values in the case of all datasets than the energy and entropy feature, as given in Table 5. In the case of various architectures of the BPNN classifier, standard deviation values of LBP-SWT decomposed sub-bands have more discriminating power to categorize multiple brain-diseased images, as shown in Table

9. For the aforementioned binary and multi-class disease classifications, Tables 6, 7 and 8 show that our proposed method, using standard deviation as a feature, is better and more robust than existing methods. Therefore, more accurate identification of brain disease can be done using the proposed brain disease descriptor (LBP-SWT + Std dev + BPNN). The LBP-SWT approach is producing better results for MR brain images than other proposed methods, when the images are rotated and translated by varying degree and co-ordinates respectively. It tells LBP-SWT feature extraction approach can be used as rotation and translation invariant transform. And, it can assist radiologists to improve the diagnostic accuracy when images are rotated and translated.

5. CONCLUSION

In this paper, the LBP-SWT approach is presented for diagnosis of MR brain Images. LBP gives details about the local structure of MR brain image while SWT coefficients provide multi-scale directional representation for brain abnormalities encoded in the extracted LBP descriptor. Energy, standard deviation, and Shannon entropy feature calculated from LBP-SWT image are tested on widely used four MR image datasets using BPNN classifier. Standard deviation¬ outperforms other features in terms of performance parameters and also in comparison with existing techniques. Standard deviation proved to be an efficient parameter in the case of LBP-SWT decomposed sub-bands of rotated and translated images also. Experimental results reveal proposed method is efficient and promising for the diagnosis of different MR brain abnormalities in clinical applications.

In this work, T2-weighted MR images are used. The proposed method can be extended to other types of MR images, like proton density, T1-weighted images. Also, the proposed algorithm can be used for the analysis of other imaging modalities like MR spectroscopic imaging (MRSI), Computed Tomography (CT) and Positron-emission tomography (PET). Feature extraction and feature selection are major tasks in the existing CAD systems which require rigorous design information. The deep learning algorithms try to extract features directly from medical images by employing their hierarchical architectures. Therefore, deep learning approach can be widely preferred to make CAD systems computationally efficient, robust which will assist radiologists.

REFERENCES

[1] Vikhe, P.S., Thool, V.R. (2016). Mass detection in mammographic images using wavelet processing and adaptive threshold technique. Journal of Medical Systems, 40(4): 82. https://doi.org/10.1007/s10916-016-0421-7

[2] Madhe, S.P., Patil, B.D., Holambe, R.S. (2018). Design of a frequency spectrum-based versatile two-dimensional arbitrary shape filter bank: Application to contact lens detection. Pattern Analysis and Applications, 23: 45-58. https://doi.org/10.1007/s10044-018-0764-6

[3] Sprawls, P. (2000). Magnetic Resonance Imaging: Principles, Methods, and Techniques. Madison: Medical Physics Publishing.

[4] Zhang, Y., Dong, Z., Wu, L., Wang, S. (2011). A hybrid method for MRI brain image classification. Expert Systems with Applications, 38(8): 10049-10053. https://doi.org/10.1016/j.eswa.2011.02.012

[5] Das, S., Chowdhury, M., Kundu, M.K. (2013). Brain MR image classification using multi-scale geometric analysis of ripplet. Progress in Electromagnetics Research, 137: 1-17. https://doi.org/10.2528/PIER13010105

[6] El-Dahshan, E.S.A., Mohsen, H.M., Revett, K., Salem, A.B.M. (2014). Computer-aided diagnosis of human brain tumor through MRI: A survey and a new algorithm. Expert Systems with Applications, 41(11): 5526-5545. https://doi.org/10.1016/j.eswa.2014.01.021

[7] Yang, G., Zhang, Y., Yang, J., Ji, G., Dong, Z., Wang, S., Feng, C., Wang, Q. (2015). Automated classification of brain images using wavelet-energy and biogeography-based optimization. Multimedia Tools and Applications, 75: 15601-15617. https://doi.org/10.1007/s11042-015-2649-7

[8] Zhang, Y., Wang, S., Dong, Z., Phillip, P., Ji, G., Yang, J. (2015). Pathological brain detection in magnetic resonance imaging scanning by wavelet entropy and hybridization of biogeography-based optimization and particle swarm optimization. Progress in Electromagnetics Research, 152: 41-58. http://doi.org/10.2528/PIER15040602

[9] Zhang, Y., Dong, Z., Liu, A., Wang, S., Ji, G., Zhang, Z., Yang, J. (2015). Magnetic resonance brain image classification via stationary wavelet transform and generalized eigenvalue proximal support vector machine. Journal of Medical Imaging and Health Informatics, 5(7): 1395-1403. https://doi.org/10.1166/jmihi.2015.1542

[10] Wang, S., Lu, S., Dong, Z., Yang, J., Yang, M., Zhang, Y. (2016). Dual-tree complex wavelet transform and twin support vector machine for pathological brain detection. Applied Sciences, 6(6): 169. https://doi.org/10.3390/app6060169

[11] Wang, S., Zhang, Y., Dong, Z., Du, S., Ji, G., Yan, J., Yang, J., Wang, Q., Feng, C., Phillips, P. (2015). Feed-forward neural network optimized by hybridization of PSO and ABC for abnormal brain detection. International Journal of Imaging Systems and Technology, 25(2): 153-164. https://doi.org/10.1002/ima.22132

[12] Zhang, Y., Dong, Z., Wang, S., Ji, G., Yang, J. (2015). Preclinical diagnosis of magnetic resonance (MR) brain images via discrete wavelet packet transform with Tsallis entropy and generalized eigenvalue proximal support vector machine (GEPSVM). Entropy, 17(4): 1795-1813. https://doi.org/10.3390/e17041795

[13] Wang, S., Phillips, P., Yang, J., Sun, P., Zhang, Y. (2016). Magnetic resonance brain classification by a novel binary particle swarm optimization with mutation and time-varying acceleration coefficients. Biomedical Engineering/Biomedizinische Technik, 61(4): 431-441. https://doi.org/10.1515/bmt-2015-0152

[14] Nayak, D.R., Dash, R., Majhi, B. (2016). Brain MR image classification using two-dimensional discrete wavelet transform and AdaBoost with random forests. Neurocomputing, 177: 188-197. https://doi.org/10.1016/j.neucom.2015.11.034

[15] Nayak, D.R., Dash, R., Majhi, B. (2017). Stationary wavelet transform and AdaBoost with SVM based pathological brain detection in MRI scanning. CNS & Neurological Disorders-Drug Targets, 16(2): 137-149. https://doi.org/10.2174/1871527315666161024142036

[16] Nayak, D.R., Dash, R., Majhi, B. (2018). Pathological brain detection using curvelet features and least squares SVM. Multimedia Tools and Applications, 77: 3833-3856. https://doi.org/10.1007/s11042-016-4171-y

[17] Khalil, M., Ayad, H., Adib, A. (2018). Performance evaluation of feature extraction techniques in MR-Brain image classification system. Procedia Computer Science, 127: 218-225. https://doi.org/10.1016/j.procs.2018.01.117

[18] Gudigar, A., Raghavendra, U., San, T.R., Ciaccio, E.J., Acharya, U.R. (2019). Application of multiresolution analysis for automated detection of brain abnormality using MR images: A comparative study. Future Generation Computer Systems, 90: 359-367. https://doi.org/10.1016/j.future.2018.08.008

[19] Nayak, D.R., Dash, R., Majhi, B. (2020). Automated diagnosis of multi-class brain abnormalities using MRI images: A deep convolutional neural network based method. Pattern Recognition Letters, 138: 385-391. https://doi.org/10.1016/j.patrec.2020.04.018

[20] Tamilarasi, R., Gopinathan, S. (2021). Inception architecture for brain image classification. Journal of Physics: Conference Series, 1964(7): 072022. https://doi.org/10.1088/1742-6596/1964/7/072022

[21] Hu, M., Zhong, Y., Xie, S., Lv, H., Lv, Z. (2021). Fuzzy system based medical image processing for brain disease prediction. Frontiers in Neuroscience, 15: 714318. https://doi.org/10.3389/fnins.2021.714318

[22] Shanker, R., Bhattacharya, M. (2021). Automated diagnosis system for detection of the pathological brain using fast version of simplified pulse-coupled neural network and twin support vector machine. Multimedia Tools and Applications, 80(20): 30479-30502. https://doi.org/10.1007/s11042-021-10937-6

[23] Isunuri, B.V., Kakarla, J. (2022). Three-class brain tumor classification from magnetic resonance images using separable convolution based neural network. Concurrency and Computation: Practice and Experience, 34(1): e6541. https://doi.org/10.1002/cpe.6541

[24] Takrouni, W., Douik, A. (2023). Deep second generation wavelet autoencoders based on curvelet pooling for brain pathology classification. Biomedical Signal Processing and Control, 83: 104675. https://doi.org/10.1016/j.bspc.2023.104675

[25] Dora, L., Agrawal, S., Panda, R., Pachori, R.B. (2024). Pathological brain classification using multiple kernel-based deep convolutional neural network. Neural Computing and Applications, 36(2): 747-756. https://doi.org/10.1007/s00521-023-09057-z

[26] Zhou, L., Wang, M., Zhou, N. (2024). Distributed federated learning-based deep learning model for privacy MRI brain tumor detection. arXiv preprint arXiv:2404.10026. https://doi.org/10.48550/arXiv.2404.10026

[27] Akter, A., Nosheen, N., Ahmed, S., et al. (2024). Robust clinical applicable CNN and U-Net based algorithm for MRI classification and segmentation for brain tumor. Expert Systems with Applications, 238: 122347. https://doi.org/10.1016/j.eswa.2023.122347

[28] Kale, V.V., Hamde, S.T., Holambe, R.S. (2019). Brain disease diagnosis using local binary pattern and steerable pyramid. International Journal of Multimedia Information Retrieval, 8: 155-165. https://doi.org/10.1007/s13735-019-00174-x

[29] Harvard Medical School. (n.d.). Database. http://www.med.harvard.edu/AANLIB.

[30] Pietikäinen, M., Hadid, A., Zhao, G., Ahonen, T. (2011). Computer Vision Using Local Binary Patterns. Springer Science & Business Media. https://doi.org/10.1007/978-0-85729-748-8

[31] Song, K.C., Yan, Y.H., Chen, W.H., Zhang, X. (2013). Research and perspective on local binary pattern. Acta Automatica Sinica, 39(6): 730-744. https://doi.org/10.1016/S1874-1029(13)60051-8

[32] Al-Berry, M.N., Salem, M.A.-M., Ebeid, H.M., Hussein, A.S., Tolba, M.F. (2016). Fusing directional wavelet local binary pattern and moments for human action recognition. IET Computer Vision, 10(2): 153-162. https://doi.org/10.1049/iet-cvi.2015.0087

[33] Khare, M., Srivastava, P., Gwak, J., Khare, A. (2018). A multiresolution approach for content-based image retrieval using wavelet transform of local binary pattern. In Asian Conference on Intelligent Information and Database Systems, Springer, Cham, pp. 529-538. https://doi.org/10.1007/978-3-319-75420-8_50

[34] Ojala, T., Pietikäinen, M., Mäenpää, T. (2000). Gray scale and rotation invariant texture classification with local binary patterns. In European Conference on Computer Vision, Springer Berlin Heidelberg, pp. 404-420. https://doi.org/10.1007/3-540-45054-8_27

[35] Zhang, Y., Ji, G., Yang, J., Wang, S., Dong, Z., Phillips, P., Sun, P. (2016). Preliminary research on abnormal brain detection by wavelet-energy and quantum-behaved PSO. Technology and Health Care, 24(s2): S641-S649. https://doi.org/10.3233/thc-161191

[36] Wang, S., Du, S., Atangana, A., Liu, A., Lu, Z. (2018). Application of stationary wavelet entropy in pathological brain detection. Multimedia Tools and Applications, 77(3): 3701-3714. https://doi.org/10.1007/s11042-016-3401-7

[37] Zhang, Y., Dong, Z., Ji, G., Wang, S. (2015). Effect of spider-web-plot in MR brain image classification. Pattern Recognition Letters, 62: 14-16. https://doi.org/10.1016/j.patrec.2015.04.016

[38] Chen, C.M., Chen, C.C., Wu, M.C., Horng, G., Wu, H.C., Hsueh, S.H., Ho, H.Y. (2015). Automatic contrast enhancement of brain MR images using hierarchical correlation histogram analysis. Journal of Medical and Biological Engineering, 35(6): 724-734. https://doi.org/10.1007/s40846-015-0096-6

[39] Bahadure, N.B., Ray, A.K., Thethi, H.P. (2017). Image analysis for MRI based brain tumor detection and feature extraction using biologically inspired BWT and SVM. International Journal of Biomedical Imaging, 2017(1): 9749108. https://doi.org/10.1155/2017/9749108

[40] Mallat, S.G. (1989). A theory for multiresolution signal decomposition: The wavelet representation. IEEE Transactions on Pattern Analysis and Machine Intelligence, 11: 674-693. https://doi.org/10.1109/34.192463

[41] Haykin, S. (1994). Neural Networks: A Comprehensive Foundation. Prentice Hall PTR.

[42] Demirhan, A., Törü, M., Güler, I. (2015). Segmentation of tumor and edema along with healthy tissues of brain using wavelets and neural networks. IEEE Journal of Biomedical and Health Informatics, 19(4): 1451-1458. https://doi.org/10.1109/jbhi.2014.2360515

[43] Bishop, C.M. (1995). Neural Networks for Pattern

Recognition. Oxford University Press.

[44] Ojha, V.K., Abraham, A., Snášel, V. (2017). Metaheuristic design of feedforward neural networks: A review of two decades of research. Engineering Applications of Artificial Intelligence, 60: 97-116. https://doi.org/10.1016/j.engappai.2017.01.013

[45] Mohsen, H., El-Dahshan, E.S.A., El-Horbaty, E.S.M., Salem, A.B.M. (2018). Classification using deep learning neural networks for brain tumors. Future Computing and Informatics Journal, 3(1): 68-71. https://doi.org/10.1016/j.fcij.2017.12.001

[46] Siddiqui, M.F., Mujtaba, G., Reza, A.W., Shuib, L. (2017). Multi-class disease classification in brain MRIs using a computer-aided diagnostic system. Symmetry, 9(3): 37. https://doi.org/10.3390/sym9030037